USGS science for a changing world
U.S. Department of the Interior
U.S. Geological Survey

Base map from Yerkes and Campbell (2005) prepared by the U.S. Geological Survey
1:100,000 Universal Transverse Mercator projection

Edited by Carolyn A. Donlin
Manuscript approved for publication October 2, 2006

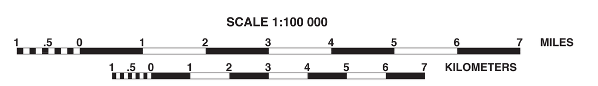

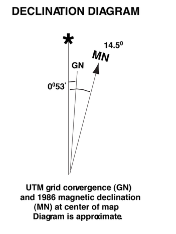

Aeromagnetic Map with Geology of the Los Angeles 30 x 60 Minute Quadrangle, Southern California

By
V.E. Langenheim, T.G. Hildenbrand, R.C. Jachens, R.H. Campbell, and R.F. Yerkes

2006

INDEX MAP

EXPLANATION

Aeromagnetic anomaly contours–Contour interval, 20 nT. Hachures indicate magnetic low. Contours were computer generated based on a 300-m grid. Blue crosses and dots are magnetization boundaries automatically calculated from grid; cross reflects greater than average magnitude of magnetic potential gradient. Dot reflects less than average magnitude of magnetic potential gradient

Model profile

Earthquake epicenter marked by focal mechanism

a — Anomaly caused by anthropogenic source–High-amplitude, short-wavelength dipole anomaly coincident with manmade features such as land fills, radio towers, or gravel pits

res — Reservoir

Fault—dashed where inferred, dotted where concealed; detachment fault denoted by hachures on hanging wall

Thrust fault—sawteeth on upper plate

LIST OF MAP UNITS

(See Yerkes and Campbell, 2005, for complete unit descriptions) Note that some units with subunits in Yerkes and Campbell (2005) have been simplified into a single unit, although internal contacts have been maintained on the map.

- Qaf — Artificial fill or graded area (late Holocene)
- Qa — Alluvium (late Holocene)
- Qb — Beach deposits (late Holocene)
- Qf — Alluvial fan (Holocene)
- Qls — Landslide deposits (Holocene and late Pleistocene?)
- Qya — Young alluvium, undivided (Holocene and late Pleistocene)
- Qw — Wash deposits (late Holocene and late Pleistocene?)
- Qyf — Young fan deposits, undivided (Holocene and late Pleistocene?)
- Qu — Undifferentiated surficial deposits (Holocene to middle Pleistocene)
- Qpv — Palos Verdes Sand (late? Pleistocene)
- Qyt — Young terrace deposits (late Pleistocene)
- Qoa — Old alluvium, undivided (late to middle Pleistocene)
- Qof — Old fan deposits, undivided (late to middle Pleistocene)
- Qsp — San Pedro Formation (middle Pleistocene)
- Qvof — Very old fan deposits, undivided (middle to early Pleistocene)
- Qpa — Pacoima Formation (middle to early Pleistocene)
- QTsb — Santa Barbara Formation (early Pleistocene)
- QTi — Inglewood Formation (early Pleistocene to late Pliocene)
- QTrx — Sedimentary rocks of the Pacific Palisades area (early Pleistocene to late Pliocene)
- QTs — Saugus Formation, undivided (early Pleistocene to late Pliocene)
- Tf — Fernando Formation, undivided (Pleistocene to Pliocene)
- Tp — Pico Formation (Pleistocene to Pliocene)
- Tw — Towsley Formation, undivided (early Pliocene and late Miocene)
- Tmt — Monterey Shale, undivided (Pliocene to Miocene)
- Tpn — Puente Formation, undivided (Miocene)
- Tm — Modelo Formation, undivided (Miocene)
- Tcs — Castaic Formation, undivided (late Miocene)
- Tmc — Mint Canyon Formation, undivided (Miocene)
- Ttk — Tick Canyon Formation,undivided (middle to early Miocene)
- Tt — Topanga Group, undivided (middle Miocene)
- Ttb — Topanga Group, basalt (middle Miocene)
- Tcb — Calabasas Formation, undivided (middle Miocene)
- Tco — Conejo Volcanics, undivided (middle Miocene)
- Ttc — Topanga Canyon Formation, undivided (middle Miocene)
- Ti — Intrusive rocks (middle Miocene)
- Trn — Rincon Formation (early Miocene)
- Tr — Trancas Formation, undivided (early and middle Miocene)
- Tz — Zuma Volcanics (early and middle MIocene)
- Tv — Vaqueros Formation (early Miocene to Oligocene)
- Tvz — Vasquez Formation, undivided (early Miocene to Oligocene)
- Tvzv — Vasquez Formation Volcanics (early Miocene to Oligocene)
- Ts — Sespe Formation, undivided (late Eocene, Oligocene, and early Miocene)
- Tcw — Coldwater Formation (late Eocene)
- Tcz — Cozy Dell Shale (Eocene)
- Tl — Llajas Formation (Eocene)
- Td — Domengine Formation (Eocene)
- Tpt — Topatopa Formation, undivided (middle to early Eocene)
- Tss — Santa Susana Formation (early Eocene to late Paleocene)
- Tlv — Las Virgenes Sandstone (Paleocene)
- Tep — Sedimentary rocks of the Chatsworth reservoir area (Eocene and/or Paleocene)
- Tmz — Martinez Formation (Paleocene)
- Tcc — Coal Canyon Formation (Eocene and Paleocene)
- Tsi — Simi Conglomerate, undivided (Paleocene)
- TKb — Sedimentary rocks in the Beverly Hills area (early Tertiary and Late Cretaceous)
- Kp — Pelona Schist (Paleocene and(or) older)
- Kc — Chatsworth Formation (Late Cretaceous)
- Kt — Tuna Canyon Formation, undivided (Late Cretaceous)
- Ktr — Trabuco Formation (Late Cretaceous)
- Kgr — Granitic rocks (Late Cretaceous)
- Kto — Tonalite, quartz diorite, and monzogranite (Late Cretaceous)
- Ktowd — Tonalite (Late Cretaceous)
- KTRogn — Mixed tonalite and Mount Lowe Granodiorite (Cretaceous and Triassic)
- Kgrm — Intimately mixed anorthosite and granite (Cretaceous and Precambrian)
- Keg — Echo granite of Miller (1930)(Cretaceous)
- Jsm — Santa Monica Slate, undivided (Late Jurassic)
- Js — Syenite (Jurassic)
- Mzbhd — Biotite-hornblende diorite (Mesozoic?)
- Mzbqd — Biotite-quartz diorite (Mesozoic?)
- Mzgd — Granodiorite (Mesozoic?)
- Mzdg — Diorite gneiss (early to middle Mesozoic)
- TRlg — Mount Lowe Granodiorite, undivided (Triassic)
- PzMzsp — Serpentinite (Mesozoic or Paleozoic)
- Pzgn — Gneiss complex (Paleozoic?)
- Pzp — Placerita Formation (Paleozoic)
- PzPms — Siliceous metasedimentary rock (Paleozoic or Proterozoic)
- Pgrp — Granite pegmatite (Proterozoic?)
- Pgn — Gneiss (Proterozoic)
- Pan — Anorthosite (Proterozoic)
- Pgb — Gabbro (Proterozoic)
- Pmg — Mendenhall Gneiss (Proterozoic)

INTRODUCTION

An important objective of geologic mapping is to project surficial structures and stratigraphy into the subsurface. Geophysical data and analysis are useful tools for achieving this objective. This aeromagnetic anomaly map provides a three-dimensional perspective to the geologic mapping of the Los Angeles 30 by 60 minute quadrangle. Aeromagnetic maps show the distribution of magnetic rocks, primarily those containing magnetite (Blakely, 1995). In the Los Angeles quadrangle, the magnetic sources are Tertiary and Mesozoic igneous rocks and Precambrian crystalline rocks. Aeromagnetic anomalies mark abrupt spatial contrasts in magnetization that can be attributed to lithologic boundaries, perhaps caused by faulting of these rocks or by intrusive contacts. This aeromagnetic map overlain on geology, with information from wells and other geophysical data, provides constraints on the subsurface geology by allowing us to trace faults beneath surficial cover and estimate fault dip and offset. This map supersedes Langenheim and Jachens (1997) because of its digital form and the added value of overlaying the magnetic data on a geologic base. The geologic base for this map is from Yerkes and Campbell (2005); some of their subunits have been merged into one on this map.

AEROMAGNETIC DATA

This aeromagnetic map is based on data from three surveys of varying resolution (table 1). Both of the onshore surveys (U.S. Geological Survey, 1980; 1996) were flown at a nominal height of 300 m (1,000 ft) above ground along flightlines spaced 0.8 to 1.6 km (0.5 to 1 mi) apart. The data were adjusted to a common magnetic datum and then merged by smooth interpolation across a buffer zone along the survey boundaries. Langenheim and Jachens (1997) published these data as a mosaic (no smoothing between surveys) at a scale of 1:100,000, and that report contains more details on how these data were processed. Most of the quadrangle is covered by the 1994-1996 detailed data (fig. 1). The smooth character of the magnetic field in the northwest and southwest corners of the map (highlighted in the color-shaded versions of the map; figs. 2 and 3) reflects the lower resolution owing to the much wider flightline spacing of the earlier two surveys.

To help delineate trends and gradients in the aeromagnetic data, we calculated magnetization boundaries in the following way: First, to emphasize the edges of shallow magnetic sources, we subtracted a numerically derived regional field from the actual merged data. The regional field was computed by analytically continuing the merged aeromagnetic data to a surface 500 m higher than that on which the measurements were made, an operation that tends to smooth the data by attenuating short-wavelength anomalies (Blakely, 1995). The resulting residual aeromagnetic field after subtracting the regional field accentuates those anomalies caused by shallow sources (< 1-2 km; fig. 3). Second, the resulting residual aeromagnetic field was mathematically transformed into magnetic potential anomalies (Baranov, 1957); this procedure effectively converts the magnetic field to the equivalent "gravity" field that would be produced if all magnetic material were replaced by proportionately dense material. This procedure assumes that the direction of the rock magnetization is parallel to the present direction of the Earth's magnetic field and does not take into account significant remanent magnetizations that are reversed or rotated relative to today's field. Third, the horizontal gradient of the magnetic potential field was calculated everywhere by numerical differentiation. Lastly, locations of the locally steepest horizontal gradient were determined numerically (Blakely and Simpson, 1986). These locations occur approximately over vertical or near-vertical contacts that separate rocks of contrasting magnetic properties and are shown as blue crosses and dots on the map.

DESCRIPTION OF AEROMAGNETIC ANOMALIES

Many magnetic anomalies of the Los Angeles quadrangle can be explained by magnetization contrasts between the surface geologic units. For example, mountainous areas with outcrops of crystalline basement rocks are generally associated with short-wavelength, high-amplitude anomalies, in contrast to the smoother anomalies present over thick sedimentary fill in the Los Angeles, San Fernando, and East Ventura Basins. Magnetic anomalies caused by Tertiary volcanic rocks and Precambrian and Mesozoic igneous and metamorphic rocks are prominent in the Verdugo, San Gabriel, and Santa Monica Mountains. The strongest, most areally extensive magnetic anomaly coincides with pre-Cenozoic crystalline basement rocks bounded by the Verdugo Fault on the southwest, by the south branch of the San Gabriel Fault and the Sierra Madre Fault on the northeast, and by the Raymond Fault on the southeast (where basement rocks are under sedimentary cover). The northwest margin of the high coincides with the Whitney Canyon Fault, although the shaded-relief aeromagnetic and residual maps show a subtle magnetic high (br on figs. 2 and 3) that continues northwest of the Whitney Canyon Fault, following the southern branch of the San Gabriel Fault (Langenheim and others, 2001). The southwest edge of this high coincides approximately with an inferred location for the southwest margin of a buried basement ridge (Yeats and others, 1994; Yeats and Stitt, 2003). Near the 1971 M 6.7 San Fernando epicenter, residual magnetic data indicate a linear magnetic feature that is aligned with the Sierra Madre Fault and extends 30 km northwest beyond the fault's mapped western terminus. The southern edge of the magnetic basement structure merges into the San Gabriel Fault near the buried basement ridge (arrows on fig. 3). Modeling suggests that the southern edge of the magnetic basement feature dips north about 60 degrees and intersects the hypocenter of the San Fernando earthquake at 13 km (fig. 4; Hildenbrand and others, 2001).

The coherent magnetic highs of the Verdugo Mountains contrast with the more varied magnetic character of the San Gabriel Mountains north of the San Gabriel Fault. This magnetic character reflects the diversity of ages and rock types in the San Gabriel Mountains; these mountains are characterized by high-amplitude, short-wavelength anomalies produced by Precambrian and Mesozoic crystalline basement rocks (fig. 2). The anomalies extend to the northwest a few kilometers northwest of basement exposures before being highly attenuated as a result of the thickening of weakly magnetic Tertiary sedimentary cover of the Soledad Basin.

In the western Santa Monica Mountains, high-amplitude, short-wavelength anomalies coincide with exposures of Miocene volcanic rocks. In the area south of the Simi Hills, these short-wavelength anomalies are superposed on a broader magnetic high (figs. 2, 3). The gradients flanking this high suggest that its source resides at a depth greater than 2-3 km. This magnetic signature contrasts with the relatively nondescript magnetic field present over the eastern Santa Monica Mountains, where basement rocks consisting of Santa Monica Slate and Mesozoic plutonic rocks are exposed. Magnetic susceptibility measurements show that these basement rocks are at most weakly magnetic (Langenheim and others, 2001; table 2). The character of the field in the eastern Santa Monica Mountains is indistinguishable from that of the Simi Hills and the San Fernando Valley.

The magnetic field over San Fernando Valley is characterized largely by low-amplitude, long-wavelength anomalies that reflect either deeply buried magnetic sources or less magnetic basement rocks underlying San Fernando Valley. However, linear, short-wavelength, generally low-amplitude (<25 nT) positive anomalies are also present (fig. 3) and reflect magnetic source rocks within the basin fill, possibly related to the volcanic rocks in the Topanga Group or to gravels of the Saugus Formation derived from the magnetic crystalline rocks exposed in the San Gabriel Mountains. Cretaceous turbidites of the Chatsworth Formation produce a pair of subtle (20 nT), east-northeast-trending anomalies (c on map and fig. 2) west of the Chatsworth Reservoir Fault in the Simi Hills, and magnetic susceptibility measurements (table 2) confirm that these Cretaceous sedimentary rocks are capable of producing such anomalies. On the other hand, dipolar, short-wavelength anomalies in the valley are generally caused by manmade features. For example, strong anomalies over manmade features (a on map) include those over gravel pits in the San Fernando Valley (lat 34° 14' N., long 118° 23' W.) and the substation and debris dam along the southern extent of the Santa Monica Mountains (lat 34° 7' N., long 118° 22' W.).

The magnetic field over the Los Angeles Basin also is marked by anomalies caused by anthropogenic sources (a on map). Prominent anomalies associated with oil fields include the northwest-trending anomaly over the Inglewood field (lat 34° 0.0' N., long 118° 22.5' W.), and the east-trending anomaly over the Montebello (lat 34° 1' N., long 118° 7' W.) field. The closely spaced, deeply penetrating well casings present in these oil fields are likely the dominant source of these anomalies, but contributions from other anthropogenic or natural sources associated with the oil fields cannot be ruled out. These short-wavelength anomalies are superposed on a broad magnetic high (LC on map, fig. 2) that coincides with the La Cienega block (Wright, 1991). Models indicate that southern boundary of the La Cienega block dips north about 70 degrees and may extend to depths of 15 km (fig. 5). The northwest edge of this anomaly appears to project beneath the Santa Monica Mountains in the footwall of the Santa Monica Fault. An equivalent of this deep magnetic basement could be the broad magnetic source in the hanging wall of the Santa Monica Fault zone south of the Simi Hills; these relations suggest a possible 35 km of left lateral cumulative offset on the Santa Monica Fault zone, compared to 40 km of offset described by Powell, 1993.

REFERENCES CITED

Baranov, V.I., 1957, A new method for interpretation of aeromagnetic maps—Pseudo-gravimetric anomalies: Geophysics, v. 22, p. 359-383.

Blakely, R.J., 1995, Potential Theory in Gravity and Magnetic Applications: Cambridge University Press, Cambridge, England, 441 p.

Blakely, R.J., and Simpson, R.W., 1986, Approximating edges of source bodies from magnetic or gravity anomalies: Geophysics, v. 51, p. 1494-1498.

Fuis, G.S., Clayton, R.W., Davis, P.M., and twelve others, 2003, Fault systems of the 1971 San Fernando and 1994 Northridge earthquakes, southern California: Relocated aftershocks and seismic images from LARSE II: Geology, v. 31, p. 171-174.

Hildenbrand, T.G., Langenheim, V.E., and Jachens, R.C., 2001, Utility of magnetic and gravity data in defining and characterizing blind thrusts in the Los Angeles, California, region: Western Meeting of the American Geophysical Union, Technical Programs and Abstracts, v. 82, no. 47, p.829.

Langenheim, V.E., Halvorson, P.F., Castellanos, E.L., and Jachens, R.C., 1993, Aeromagnetic map of offshore southern California borderland east of the Patton Escarpment: U.S. Geological Survey Open-File Report 93-520, scale 1:500,000.

Langenheim, V.E., and Jachens, R.C., 1997, Aeromagnetic map of the Los Angeles 1:100,000-scale quadrangle, California: U.S. Geological Survey Open-File Report 97-162.

Langenheim, V.E., Hildenbrand, T.G., Jachens, R.C., and Griscom, A., 2001, Geophysical setting of the San Fernando basin, southern California: AAPG Pacific Section Guidebook GB 77, p. 37-54.

Miller, W.J., 1934, Geology of the western San Gabriel Mountains of California: Berkeley, University of California Department of Geological Sciences Bulletin, v. 17, p. 193-240.

Mori, James, Wald, D.J., and Wesson, R.L., 1995, Overlapping fault planes of the 1971 San Fernando and 1994 Northridge, California earthquakes: Geophysical Research Letters, v. 22, no. 9, p. 1033-1036.

Powell, R.E., 1993, Balanced palinspastic reconstruction of pre-late Cenozoic paleogeology, southern California: Geological Society of America Memoir, p. 1-106.

U.S. Geological Survey, 1996, Aeromagnetic map of parts of the Los Angeles, Long Beach, and adjacent 1 x 2 degree quadrangles, California: U.S. Geological Survey Open-File Report 96-550, scale 1:250,000.

U.S. Geological Survey, 1980, Aeromagnetic map of the Ventura Basin, Ventura and Los Angeles counties, California: U.S. Geological Survey Open-File Report 80-64, scale 1:62,500.

Whitcomb, J.H., Allen, C.R., Garmany, J.D., and Hileman, J.A., 1973, San Fernando earthquake series, 1971—Focal mechanisms and tectonics: Review of Geophysics, v. 11, p. 693-730.

Wright, T.L, 1991, Structural geology and tectonic evolution of the Los Angeles basin, California: in K.T. Biddle, ed., Active Margin Basins, p. 35-134.

Yeats, R.S., Huftile, G.J., and Stitt, L.T., 1994, Late Cenozoic tectonics of the East Ventura basin, Transverse Ranges, California: American Association of Petroleum Geologists Bulletin, v. 78, p. 1040-1074.

Yeats, R.S., and Stitt, L.T., 2003, Ridge Basin and San Gabriel fault in the Castaic lowland, southern California: Geological Society of America Special Paper 367, p. 131-155.

Yerkes, R.F., and Campbell, R.H., compilers, 2005, Preliminary geologic map of the Los Angeles 30' x 60' quadrangle, southern California: U.S. Geological Survey Open-File Report 2005-1019, map scale 1:100,000.

Table 1. Surveys used to create aeromagnetic map.

Survey	Year Flown	Flight elevation above ground	Flightline spacing	Flightline direction
Los Angeles (U.S. Geological Survey, 1996)	1994-6	305 m	0.8 km	N/S
Ventura Basin (U.S. Geological Survey, 1980)	1977	305 m	3.2 km	N/S
Offshore Southern California	1961	760 m*	1.6 km	NE/SW

*flight elevation estimated

Table 2. Magnetic susceptibilities of rocks in the Los Angeles quadrangle. N, number of samples.

	Magnetic susceptibility (10^{-3} cgs units) Average±standard deviation	Range	N
Crystalline rocks			
Verdugo Mountains	0.76±0.64	0.00-2.75	33
San Gabriel Mountains (South of SGF*)	0.76±1.02	0.00-3.69	22
San Gabriel Mountains (North of SGF)	1.08±2.07	0.00-7.37	22
Santa Monica Mountains:			
Slate & plutonic rocks	0.01±0.01	0.00-0.02	16
Simi Hills Cretaceous rocks	0.15±0.17	0.01-0.61	27
Tertiary volcanic rocks	0.44±0.33	0.01-2.13	79
Tertiary sedimentary rocks	0.03±0.05	0.00-0.20	13

*SGF, south branch of San Gabriel Fault.

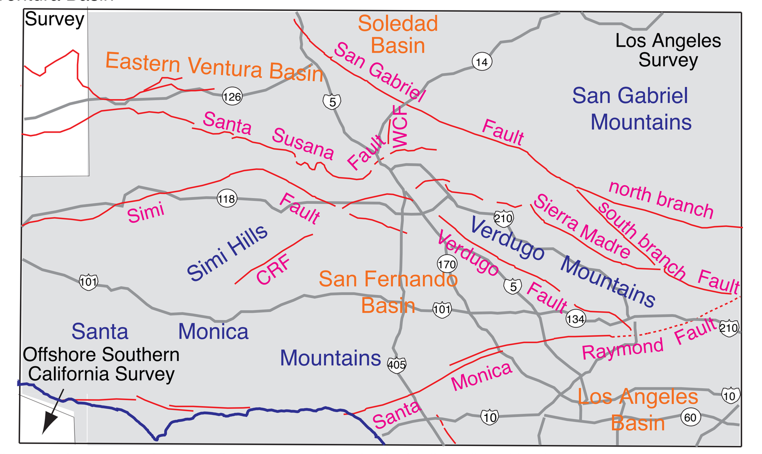

Figure 1. Aeromagnetic survey index map with major faults (in red) and basins. Gray area is covered by 1994-1996 detailed aeromagnetic survey. Dark gray lines are major highways. CRF, Chatsworth Reservoir Fault; WCF, Whitney Canyon Fault.

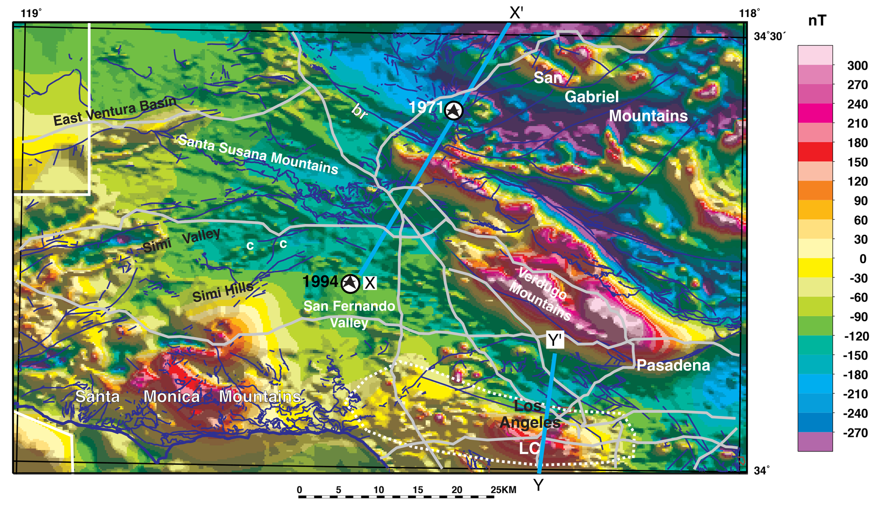

Figure 2. Color-shaded contour aeromagnetic anomaly map of the Los Angeles 30 x 60 minute quadrangle. Color contour interval, 30 nT. Illumination is from the northeast, highlighting northwest-striking features. Gray lines are major highways. White lines mark survey boundaries. Dark blue lines are faults from Yerkes and Campbell (2005). LC refers to La Cienega broad magnetic high approximately outlined by dashed white line. c refers to anomaly caused by Cretaceous sedimentary rocks. br is basement ridge. Blue lines are model profile locations. Stars are 1971 San Fernando and 1994 Northridge earthquake epicenters.

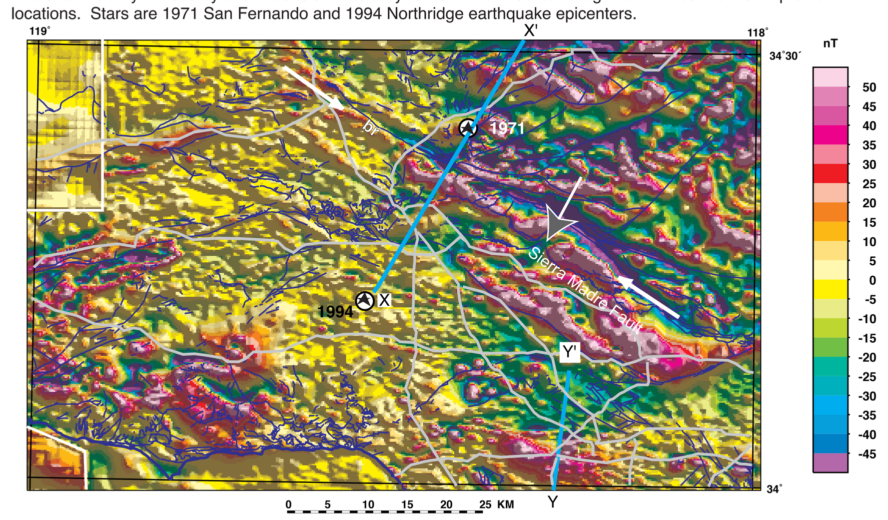

Figure 3. Color-shaded contour residual aeromagnetic map of the Los Angeles 30 x 60 minute quadrangle. Color contour interval, 5 nT. Gray lines are major highways (see fig. 1). White lines mark survey boundaries. Dark blue lines are faults. Blue lines are model profile locations. br is basement ridge. White arrows point to Sierra Madre magnetic anomaly; white-outlined gray arrow points to western mapped terminus of the Sierra Madre Fault. Stars are 1971 San Fernando and 1994 Northridge earthquake epicenters.

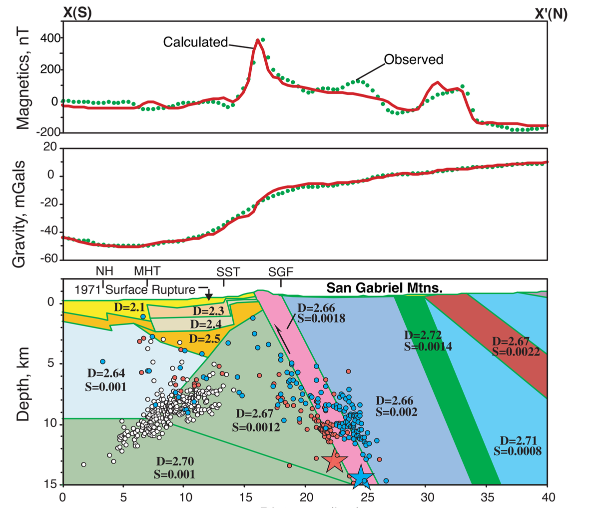

Figure 4. Magnetic and gravity model along profile X-X' that illustrates the geometry of the basement feature aligned with the Sierra Madre Fault. Blocks in model are defined by density (D, in g/cm³) and magnetic susceptibility (S, in cgs units). NH, Northridge Hills Fault; MHT, Mission Hills thrust; SST, Santa Susana thrust; SGF, San Gabriel Fault. Star marks hypocenter of 1971 San Fernando mainshock (red from Whitcomb and others, 1973; blue from Fuis and others, 2003). Small red circles, aftershocks of the 1971 mainshock; white circles, aftershocks of the 1994 Northridge mainshock from Mori and others (1995); blue circles, aftershock locations of the 1971 mainshock in Fuis and others (2003) .

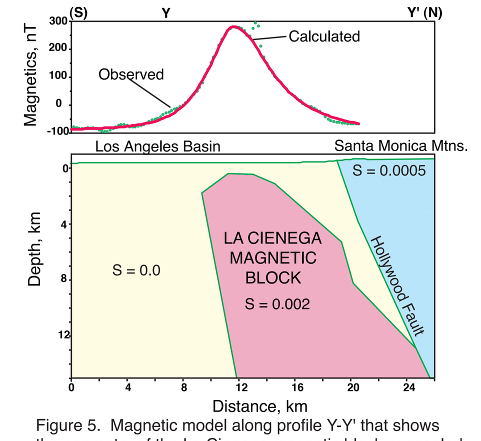

Figure 5. Magnetic model along profile Y-Y' that shows the geometry of the La Cienega magnetic block concealed beneath the Los Angeles Basin sediments. Y marks the southern edge of the 30 x 60 minute quadrangle. S, magnetic susceptibility in cgs units.

For sale by U.S. Geological Survey, Information Services, Box 25286, Federal Center, Denver, CO 80225, 1-888-ASK-USGS

Digital files available at http://pubs.usgs.gov/sim/2006/2950/